Overcoming photon blockade in a circuit-QED single-atom maser with engineered metastability and strong coupling

A. A. Sokolova [1,2,3,4] D. A. Kalacheva [5,2,3,1] G. P. Fedorov [1,2,3,*] and O. V. Astafiev [5,2]

[1]*Superconducting Quantum Circuits group, Russian Quantum Center, 121205 Skolkovo village, Russia*
[2]*Laboratory of Artificial Quantum Systems, Moscow Institute of Physics and Technology, 141701 Dolgoprudniy, Russia*
[3]*Laboratory of Superconducting Metamaterials, National University of Science and Technology MISIS, 119049 Moscow, Russia*
[4]*Quantum Integrated Devices group, Institute of Science and Technology Austria, 3400 Klosterneuburg, Austria*
[5]*Center for Engineering Physics, Skolkovo Institute of Science and Technology, 121205 Moscow, Russia*

Reaching a high cavity population with a coherent pump in the strong-coupling regime of a single-atom laser is impossible due to the photon blockade effect. In this Letter, we experimentally demonstrate that in a single-atom maser based on a transmon strongly coupled to two resonators, it is possible to pump over a dozen photons into the system. The first high-quality resonator plays the role of a usual lasing cavity, and the second one presents a controlled dissipation channel, bolstering population inversion, and modifies the energy-level structure to lift the blockade. As confirmation of the lasing action, we observe conventional laser features such as a narrowing of the emission linewidth and external signal amplification. Additionally, we report unique single-atom features: self-quenching and several lasing thresholds.

I. INTRODUCTION

Experimental studies on single-atom lasers and masers are following the recent developments in the quantum optics of individual quantum systems [1]. Trapped atoms/ions [2,3], superconducting artificial atoms [4–7], semiconductor double quantum dots [8–10], and biased Josephson junctions [11] have already been used as a single-atom gain medium and allowed experimental investigations of nonconventional properties of these lasers such as multistability, emission of squeezed radiation, self-quenching, etc. For contemporary superconducting artificial atoms featuring high coherence (transmon and fluxonium types), it is not obvious how to directly implement incoherent pumping and achieve population inversion. Coherent pumping, in contrast, is prohibited for strongly coupled systems due to the photon blockade [12–14]. Recently, there was a theoretical proposal [15] regarding a superconducting circuit-QED [16] maser consisting of a magnetic-flux-tunable Xmon-type transmon [17] coupled to two microwave resonators: a high-Q reservoir to accumulate microwave photons, and a low-Q auxiliary one. The latter cavity forms an engineered dissipative environment enforcing metastability of the second excited transmon state. Besides bolstering the population inversion, it also significantly modifies the maser energy-level structure and allows it to overcome the photon blockade, limiting the intensity of the emitted radiation in coherently pumped systems with strong coupling [12,13]. A physical realization of the proposed device would allow one to assess experimentally the viability of the architecture which may be of use also

in different applications [18] and to study those properties that cannot be explored in numerical simulations, for example, the spectrum of the emitted radiation which is hard to compute [19]. Additionally, we expect that the suggested architecture will be suitable for different quantum devices, for example, coherent quantum phonon emitters, which have a wide range of both scientific and practical applications [20]. In this Letter, we describe our implementation of the suggested architecture and present the main results confirming the lasing action of the device.

II. DEVICE

In Fig. 1(a), we reproduce the conceptual schematic of the device from the proposal [15]. The system includes a transmon qubit with energy levels shown in red and marked as $|g, e, f\rangle$, the auxiliary resonator in yellow with its two lowest levels denoted as $|0, 1\rangle_a$, and the reservoir (lasing) resonator in blue whose levels $|N - 1, N\rangle_r$ are also shown. To observe lasing, one needs to ensure population inversion of the $|g, e\rangle$ subspace. When two-photon pumping $|g\rangle \rightrightarrows |f\rangle$ is employed, this means that the relaxation rate $|f\rangle \rightarrow |e\rangle$ should necessarily be much higher than the rate $|e\rangle \rightarrow |g\rangle$. For a bare transmon the ratio between these rates is $\Gamma_{fe}/\Gamma_{eg} \approx 2$ [21,22], which was shown to be not enough [15]. A solution is to enhance the $|f\rangle$-state decay by opening a resonant dissipative channel via coupling the transmon to a low-Q auxiliary cavity. Rather unexpectedly, this approach is also predicted to fulfill the resonance condition for a coherent pump at high reservoir populations N_{ss} which would otherwise become ineffective due to the growing transmon-reservoir Rabi splittings (see the detailed discussion in the proposal [15]).
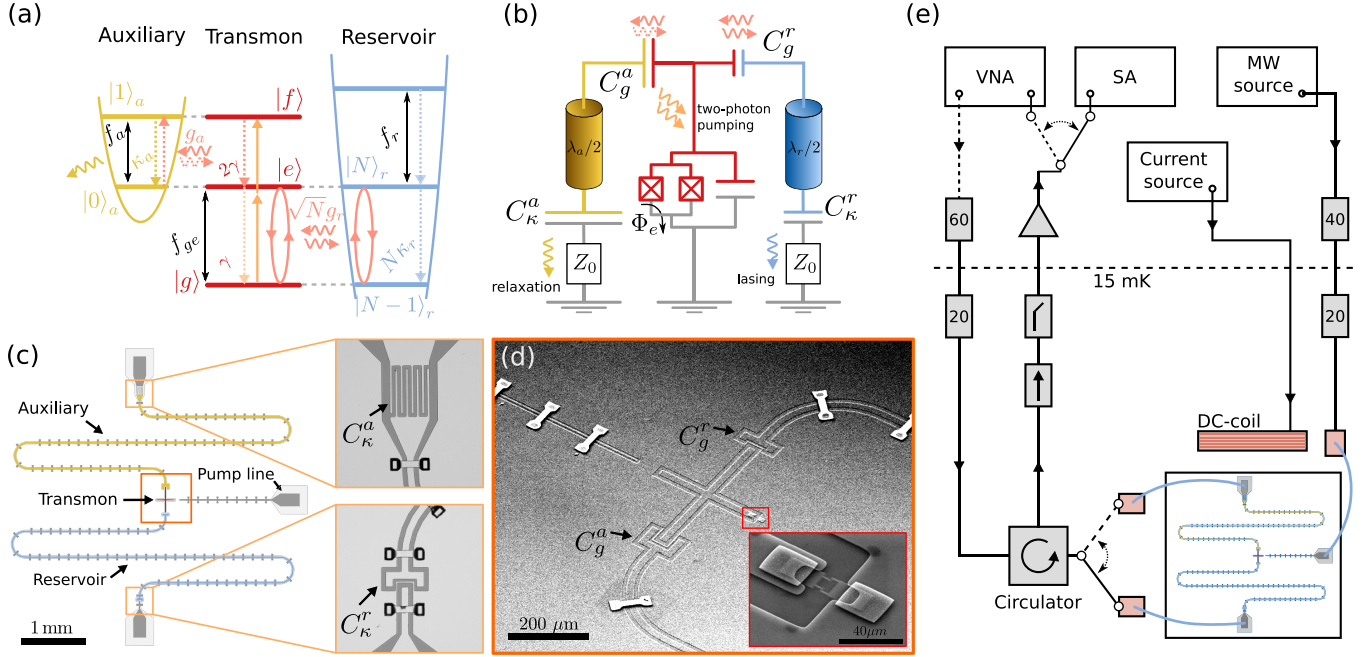
*gleb.fedorov@phystech.edu

FIG. 1. (a) A scheme showing the configuration of the energy levels when the reservoir is resonant with the $|g\rangle \leftrightarrow |e\rangle$ transition, and the auxiliary cavity is resonant with the $|e\rangle \leftrightarrow |f\rangle$ transition. (b) Schematic of the circuit-QED implementation of the system. To the left is the auxiliary and to the right is the reservoir cavity, implemented as half-wave transmission line (coplanar waveguide) resonators. Capacitors $C_g^{r,a}$ couple the transmon to the reservoir, an auxiliary cavity; $C_\kappa^{r,a}$ define the desired external quality factors. (c) Design of the device (photolithography layer) and optical images of the cavity coupling capacitors. Microwave antenna routing the pump signal towards the transmon comes from the right-hand side of the sample. The colors of the elements correspond to the colors on (a) and (b). (d) SEM image of the transmon coupled to the cavities; in the inset, the SQUID area is shown with a higher magnification. (e) Scheme of measurement: The sample as in (c) is wire bonded, refrigerated to 15 mK, the input signals coming through attenuated coaxial lines, and the output line containing an amplifier chain with a high-electron mobility transistor (HEMT) amplifier. With one switch, one chooses whether to measure the reflection off the auxiliary or reservoir resonator, and with another the signal analyzer (SA) and vector network analyzer (VNA) are exchanged; an external solenoid supplies a dc magnetic field to the SQUID.

The Hamiltonian of the system in the laboratory frame reads,

$$\hat{H} = \hat{H}_t + \sum_{\lambda=r,a} \left(\hat{H}_c^{(\lambda)} + \hat{H}_i^{(\lambda)} \right), \tag{1}$$

$$\hat{H}_t = h f_{ge}^{max} b^\dagger b + \frac{h\alpha}{2} b^\dagger b (b^\dagger b - 1), \tag{2}$$

$$\hat{H}_c^{(\lambda)} = h f_{(\lambda)} (a_\lambda^\dagger a_\lambda + 1/2), \tag{3}$$

$$\hat{H}_i^{(\lambda)} = \hbar g_\lambda (b a_\lambda^\dagger + b^\dagger a_\lambda), \tag{4}$$

where $\hat{H}_t$, $\hat{H}_c^{(\lambda)}$, and $\hat{H}_i^{(\lambda)}$ are the transmon, cavity, and interaction Hamiltonians, and where $a_{r,a}, b$ are the bosonic annihilation operators for the reservoir, auxiliary resonator, and transmon. The cavities are designed to have coupling strengths $g_{r,a}$ and leakage rates $\kappa_{r,a}$. The design values for these parameters have been optimized using a standard numerical algorithm for maximal steady-state reservoir emitter power, which corresponds to around $N_{ss} = 50$ photons in the reservoir [15]. The relevant Gorini-Kossakowski-Sudarshan-Lindblad (GKSL) master equation is based on the collapse operators $\sqrt{\kappa_{r,a}} a_{r,a}$, $\sqrt{\gamma} b$ for the relaxation of the cavities and the transmon and $\sqrt{\gamma_\phi} b^\dagger b$ for the pure dephasing of the transmon. For comparison between the design parameters and the parameters found experimentally in this Letter, along with a brief description of their meaning, see Table I. In the proposal [15] we have established that the system is rather

resilient to deviations in the parameters, and the experimental values are close enough to the optimal ones for the high-N_{ss} lasing to be possible, which we confirm numerically [23]. The transmon frequency is maximal for zero external flux through its SQUID loop (around 5.95 GHz) and can be tuned down in frequency into resonance with the reservoir and auxiliary cavity, consecutively. Using an approximation [24],

$$f_{ge}(\Phi_e) \approx f_{ge}^{max} \sqrt{\cos(\pi \Phi_e / \Phi_0)}, \tag{5}$$

TABLE I. Summary of the device parameters, measured versus planned in the design. Associated with dielectric loss, the reservoir total decay rate κ_r depends strongly on the measurement power, and the highest value is given here.

Parameter	Meaning	Measured	Design
f_r	Reservoir cavity frequency	5.860 GHz	6 GHz
κ_r	Res. total decay rate	0.69 μs^{-1}	0.31 μs^{-1}
κ_r^e	Res. decay rate to feedline	0.3 μs^{-1}	0.31 μs^{-1}
$g_r/2\pi$	Res.-transmon coupling	11 MHz	6.5 MHz
f_a	Auxiliary cavity frequency	5.715 GHz	5.8 GHz
κ_a	Aux. total decay rate	90 μs^{-1}	138 μs^{-1}
$g_a/2\pi$	Aux.-transmon coupling	15.5 MHz	23.5 MHz
f_{ge}^{max}	Zero-flux transmon frequency	5.95 GHz	6.5 GHz
α	Transmon anharmonicity	180 MHz	200 MHz
$f_r - f_a$	Res.-aux. cavity detuning	145 MHz	200 MHz

where Φ_e/Φ_0 is the ratio of the external flux through the SQUID to the magnetic flux quantum. There is a discrepancy between the anharmonicity of the transmon and the frequency difference between the cavities (180 vs 145 MHz), and appreciable deviations in κ_a and g_a from design values. This mismatch does not critically affect the functioning of the device by virtue of the general robustness of the optimal N_{ss} to parameter perturbations for large values of κ_a (see Ref. [15], Sec. II). The most important deviation from the optimized parameters, though, is the non-negligible internal loss of the reservoir cavity which we estimate from the fit to be $\kappa_r^i = \kappa_r - \kappa_r^e = 0.39\ \mu s^{-1}$ in the worst case (see Supplemental Material [23]). As N_{ss} in the simple model is inversely proportional to total reservoir loss [15], and as the internal loss in our case approximately equals the external, one can expect halving of the device maximum emission intensity compared to the ideal case. We take κ_r^e into account when calculating the N_{ss} from the measured signal power. Finally, we note that the proper relaxation and coherence times of the transmon were not measured directly due to the limitations of the experimental setup; one can expect its relaxation rate to be lower than κ_r^i due to a lower interface participation ratio [25], while the dephasing can be neglected as the system functions in a mixed state [15].

The electrical scheme of the device and the design for nanofabrication are shown in Figs. 1(b) and 1(c). The couplings and dissipation rates are physically determined by the capacitances $C_{\kappa,g}^{a,r}$ which are small enough to be produced in a single Al layer. However, as they break the ground plane, we also use air bridges to ensure the uniformity of the ground electric potential. In Fig. 1(d) we show a scanning electron microscopy (SEM) image of the Xmon along with its superconducting quantum interference device (SQUID) in the inset (see Supplemental Material [23] for fabrication details).

III. REFLECTION AND EMISSION SPECTROSCOPY

We begin the study of the system in its working point $\Phi_e^* > 0$ when the transmon is tuned into resonance with the reservoir, $f_{ge}(\Phi_e^*) = f_r$. We first perform reflection spectroscopy of the reservoir resonator [see Fig. 2(a)]. The vector network analyzer (VNA) measuring the complex reflection parameter S_{11} is set to a low power near the single-photon regime for the reservoir cavity (the frequency sweep range of the VNA is shown on the y axis). While performing spectroscopy, we send an additional signal at $f_p = f_{gf}/2 = 5.788\ \text{GHz}$ to the pump line using a separate microwave source. Its power is shown on the x axis. When its power is off or very low, two transitions of the avoided crossing $|0_a, g, 0_r\rangle \rightarrow (|0_a, g, 1_r\rangle \pm |0_a, e, 0_r\rangle)/\sqrt{2}$ are visible at 5.854 and 5.876 GHz, from which $g_r/2\pi = 11\ \text{MHz}$ (see Supplemental Material [23]). When the two-photon pumping power is increased, these transitions become shifted upwards in frequency (this is probably connected with the light-dressing effects in composite systems [26,27]) and saturate. They completely disappear at around the -10 dBm level of the microwave source, which is the beginning of the lasing action. The $|S_{11}|$ characteristic of the remaining spectral line is not a Lorentzian dip above this power but shows small amplification—a manifestation of the injection locking effect
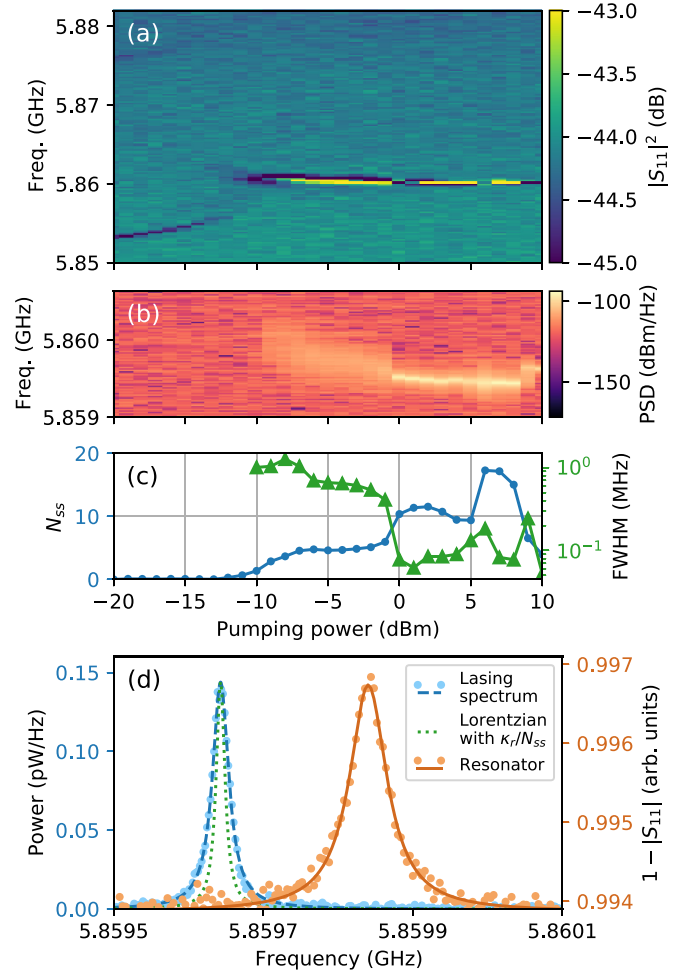

FIG. 2. (a) Reflection spectroscopy of the transmon-resonator avoided crossing vs the two-photon pumping power, pumping frequency $f_p = 5.788\ \text{GHz}$, where the VNA signal power is at -50 dBm, $\Phi_e = \Phi_e^* : f_{ge}(\Phi_e^*) = f_r$. (b) Measured emission spectrum from the reservoir cavity vs the pumping power. (c) Estimated number of photons in the reservoir N_{ss} (blue dots) and the spectral linewidth calculated from (b) by Lorentzian fitting (green triangles). (d) Lasing spectrum (light-blue dots for data and blue dashed line for fit, FWHM: 26 kHz) for 10-dBm pumping power data compared with the resonator reflection profile for the same photon population ($N_{ss} = 3.9$, orange dots for data and orange line for fit, 61 kHz) and the Schawlow-Townes limit (green dotted line, 16 kHz).

[28]. Also, above -10 dBm the reservoir begins to emit power [Fig. 2(b)] which can be detected upon disconnecting the VNA from the measurement setup and connecting a signal analyzer (SA) to the output line.

Precise calibration of the emission power is difficult due to the uncertainty of the amplification level in the output line. We find it by using the fact that each branch of the vacuum Rabi splitting can be regarded as an effective two-level system, for which the calibration of absolute input power is feasible [29,30]. First, we measure the saturation of the avoided crossing peaks with an increase of VNA power P_{VNA} and compare the data with a numerical simulation for the extracted system parameters; this allows us to find the driving amplitude, and thus the absolute signal power $P_{c.p.}$ at the reservoir coupling

port for a given P_{VNA}. Next, we measure the power of a slightly off-resonant reflected and amplified signal P_{SA} by the SA assuming almost unity reflection off the coupling port in the vicinity of the resonance. Finally, we calculate the amplification level $a = P_{\text{SA}}/P_{\text{c.p.}}$ in the output line (see details in the Supplemental Material [23]). When the amplification is known, the total emission power at the coupling port can be calculated as an integral of the signal power spectral density $S_{VV}(f)$ measured by the signal analyzer as

$$P = \kappa_r^e N_{\text{ss}} \hbar \omega = \frac{1}{a} \int_{\text{BW}} S_{VV}(f) df, \qquad (6)$$

where BW stands for the bandwidth where the emission signal is non-negligible. For this value, we take the span of the SA shown on the y axis of Fig. 2(b). We plot the calibrated N_{ss} versus pumping power in Fig. 2(c) and confirm that it is indeed possible to achieve significant reservoir population using our architecture: In the range between 5 and 10 dBm of pumping power, the reservoir accumulates nearly 20 photons. According to the model described in the proposal and generalized to the case of nonzero detuning between the transitions $e \rightarrow f$ and $|0\rangle_a \rightarrow |1\rangle_a$, for experimental parameters the system should accumulate around 24 photons, which is in good agreement with the data. Using a numerical model with the experimental parameters, we find even better agreement for maximal N_{ss} around 19 (for details on both approaches, see Supplemental Material [23]).

In Fig. 2(c), one can observe four lasing thresholds in N_{ss} located at -10, -1, 5, and 8 dBm which are accompanied by changes in the emission linewidth and lasing frequency. This behavior is probably connected with the special energy-level structure of the system [15] and can be qualitatively reproduced in simulations (see Supplemental Material [23]). After the last threshold, there is a significant decrease of N_{ss}, which we identify as the self-quenching effect [31].

Finally, in Fig. 2(d) we compare the lasing spectrum and reservoir cavity response, which both can be well approximated by Lorentzian curves. The orange line shows $1 - |S_{11}|$ when the transmon is far detuned, and the blue line is the lasing spectrum at 10 dBm pumping power. The central frequency of the latter is 200 kHz lower than f_r, which may be explained by the fact that frequencies of the transitions between high-energy levels are not equal to f_r due to strong coupling [15]. For high reservoir population, the line of the emission spectrum is significantly narrower than the resonator proper amplitude characteristic: The full width at half maximum (FWHM) is 26 vs 61 kHz for $N_{\text{ss}} = 3.9$, and approaches the Schawlow-Townes-limited spectrum with a width of $\kappa_r/2\pi N_{\text{ss}} = 16$ kHz.

As an additional test for the laser action of the device, we show that an external microwave signal is amplified upon reflection off the reservoir cavity when the system is pumped above the first threshold. The results are presented in Fig. 3 for three different pumping powers: -5 dBm [Fig. 3(a)], 5 dBm [Fig. 3(b)], and 10 dBm [Fig. 3(c)]. The reference level is $G = 1$, and the dip in the data trace means resonant absorption of radiation, while the peak reveals amplification. Amplification depends nonlinearly on the pumping power, with a maximum amplitude gain of $G \approx 3$ at 5 dBm pumping power. In Fig. 3(d), one can see how the amplification saturates with
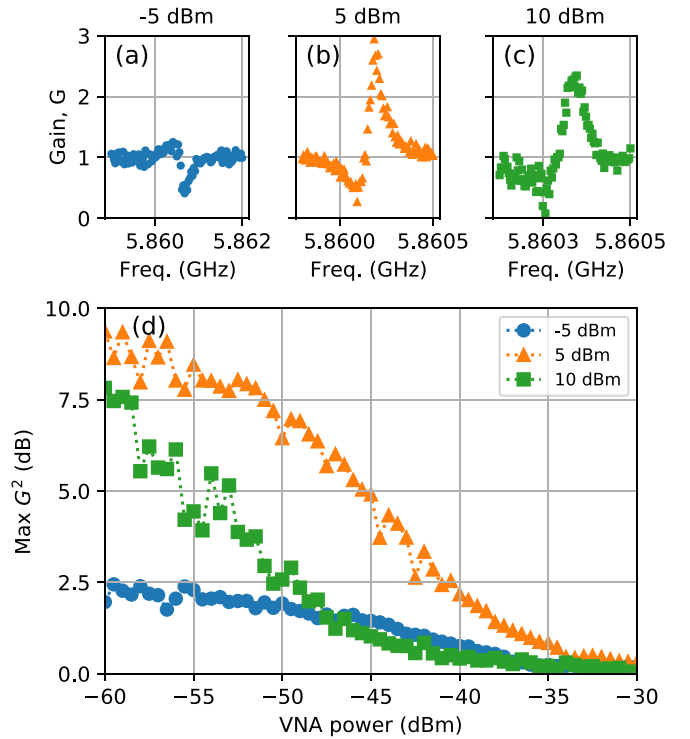

FIG. 3. (a)–(c) Gain of reflection amplitude vs frequency for pumping powers -5 (blue circles), 5 (orange triangles), and 10 dBm (green squares), respectively, at a VNA power of -60 dBm, $\Phi_e = \Phi_e^*$. (d) Maximum value of the power gain over the frequency range shown on the x axes in (a)–(c) depending on the VNA power for three pumping powers.

increased VNA power for the three values of pumping power, which is a typical behavior [28]. We also observe that in Fig. 3(a) the shape of the curve has an amplification area below a dip in frequency, while in Figs. 3(b) and 3(c) it is slightly above. Based on the data shown in Fig. 2(a), we find that the transition between these regimes occurs at 0 dBm of pumping power, and it coincides with the second lasing threshold in Fig. 2(c); the nature of this effect remains unclear to us.

In order to quantify the device action outside the optimal regime and better understand the lasing mechanism, we also study the dependence of the emission spectrum on the external flux in the SQUID and pumping frequency. We now use lower-power pumping (-5 dBm) to avoid power broadening and achieve better resolution of the transitions. Figure 4(a) shows a scan of two symmetric avoided crossings with vertical solid lines marking the points where the transmon ge transition is resonant with the reservoir (at Φ_e^*), and dashed lines where the ge transition is resonant with the pump signal. The first configuration was studied before in Fig. 1(a), and in the second one the qubit may be pumped directly. As can be seen in Figs. 4(b) and 4(c), the reservoir population is the highest in proximity to the solid lines, both in the experiment and the simulation. It is clearly visible, however, that in the simulation for the experimental parameters a maximum population is reached for $|\Phi_e| < \Phi_e^*$. We also note that emission is observed for a wider frequency range in the experiment than in the simulation. A small dip in N_{ss} which coincides with the central points of the
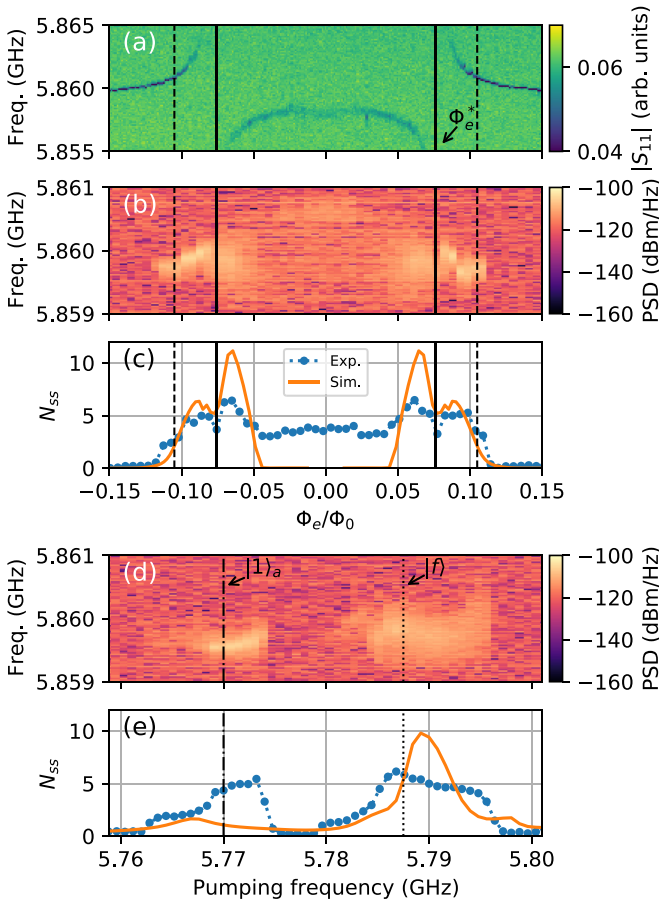
FIG. 4. (a) Reflection spectroscopy of the avoided crossing at -60 dBm on the VNA vs magnetic flux Φ_e through the transmon SQUID. Vertical solid lines mark the points of transmon-reservoir resonance and vertical dashed lines show Φ_e^* where the ge frequency is equal to the pumping frequency. (b) Lasing spectrum vs Φ_e for a pumping power of -5 dBm at 5.788 GHz. (c) Reservoir N_{ss}: Experiment (blue dots) and simulation (orange curve) vs Φ_e. (d) Lasing spectrum depending on the pump frequency when its power is -5 dBm. The dashed-dotted line shows the two-photon frequency of the $|g\rangle \rightleftarrows |1\rangle_a$ process, and the dotted line the $|g\rangle \rightleftarrows |f\rangle$ process. (e) Number of photons in the reservoir resonator vs pumping power: Experiment (blue dots) and simulation (orange curve).

avoided crossings can be explained by the fact that low-power pumping cannot overcome the photon blockade, being under the lasing threshold [15].

Similarly, we measure the dependence of the emission spectrum on the pumping frequency for the resonant configuration. The results are shown in Fig. 4(d). Since there is a 35 MHz detuning between $f_r + f_a$ and f_{gf} when $f_{ge} = f_r$, we mark two competing cases of two-photon pumping: The dashed-dotted vertical line corresponds to the resonance with the transition from the ground state to $|1_a, e, 0_r\rangle$ (this is the configuration chosen in Fig. 2), and the dotted one to $|0_a, f, 0_r\rangle$. In Fig. 4(e), two areas of high emission attributed to these processes are clearly visible. We find that in contrast with the simulation, in the experiment both pumping frequencies give comparable values for the integrated emission power and the corresponding photon number in the reservoir; however, pumping at $f_{gf}/2$ gives a wider emission line than

at $(f_r + f_a)/2$. We also note the asymmetry of the emission areas with respect to the corresponding marker lines, showing a notable shift towards higher pump frequencies.

IV. DISCUSSION

In this Letter, we have implemented a single-atom maser based on a transmon that overcomes the photon blockade in the strong-coupling regime, concluding a previous theoretical study on the subject and continuing the preceding works employing the superconducting artificial atoms [5,7]. We have shown experimentally the possibility to reach more than 15 photons in a cavity, a notably high population for a coherent pump in this class of systems [3,12,13,15]. Additionally, we found that the system demonstrates complex behavior, exhibiting several lasing thresholds and self-quenching accompanied by variations in the emission spectrum central frequency and linewidth while usually single-atom lasers in the strong-coupling regime are thresholdless [2,3,32].

We explain the possibility to overcome the photon blockade in our device by the additional splittings in the level structure emerging from coupling to an auxiliary resonator and ensuring a resonance condition for the two-photon pump for high populations. Our theoretical studies predict that the studied system should exhibit such features as bistability of the Wigner function and sub-Poissonian statistics of emitted radiation [15]; however, further experimental study on this subject is required as we could not yet study those effects due to technical limitations.

Along with an experimental study of this kind of a device, we have also investigated in more detail the conventional manifestations of the lasing effect to confirm its nature. First, we have demonstrated that the emission linewidth is narrower than the resonator proper linewidth and, notably, approaches the Schawlow-Townes limit for certain regimes. Second, if supplied, an external microwave signal is being amplified by the device; this effect was previously demonstrated for single-atom masers [4] as well as in ordinary lasers and is caused by the injection-locking effect [28]. We note, however, that while our measurements of the injection-locking effect in the studied device exhibited an expected line narrowing around the injected signal [23], we could not obtain data similar to what was shown in recent works [11,33] with the injection signal detuned. This may be due to the fact that in contrast to those works we employ coherent pumping and the lasing cavity population is not very large in our case (i.e., compared to $N_{ss} = 3 \times 10^4$ in Ref. [11]).

Finally, we measured the emission spectrum depending on the transmon frequency and pumping frequency and observed that lasing manifests itself when the system parameters are close to the theoretically predicted ones, which is strong evidence of the correctness of our model.

[1] S. Haroche and J.-M. Raimond, *Exploring the Quantum: Atoms, Cavities, and Photons* (Oxford University Press, Oxford, UK, 2006).

[2] J. McKeever, A. Boca, A. D. Boozer, J. R. Buck, and H. J. Kimble, Nature (London) **425**, 268 (2003).

[3] F. Dubin, C. Russo, H. G. Barros, A. Stute, C. Becher, P. O. Schmidt, and R. Blatt, Nat. Phys. **6**, 350 (2010).

[4] O. Astafiev, K. Inomata, A. Niskanen, T. Yamamoto, Y. A. Pashkin, Y. Nakamura, and J. S. Tsai, Nature (London) **449**, 588 (2007).

[5] P. Neilinger, M. Rehák, M. Grajcar, G. Oelsner, U. Hübner, and E. Il'ichev, Phys. Rev. B **91**, 104516 (2015).

[6] P. Neilinger, S. N. Shevchenko, J. Bogár, M. Rehák, G. Oelsner, D. S. Karpov, U. Hübner, O. Astafiev, M. Grajcar, and E. Il'ichev, Phys. Rev. B **94**, 094519 (2016).

[7] O. V. Astafiev, A. A. Abdumalikov, A. M. Zagoskin, Y. A. Pashkin, Y. Nakamura, and J. S. Tsai, Phys. Rev. Lett. **104**, 183603 (2010).

[8] M. Nomura, N. Kumagai, S. Iwamoto, Y. Ota, and Y. Arakawa, Nat. Phys. **6**, 279 (2010).

[9] Y. Y. Liu, K. D. Petersson, J. Stehlik, J. M. Taylor, and J. R. Petta, Phys. Rev. Lett. **113**, 036801 (2014).

[10] Y.-Y. Liu, J. Stehlik, C. Eichler, X. Mi, T. R. Hartke, M. J. Gullans, J. M. Taylor, and J. R. Petta, Phys. Rev. Lett. **119**, 097702 (2017).

[11] M. C. Cassidy, A. Bruno, S. Rubbert, M. Irfan, J. Kammhuber, R. N. Schouten, A. R. Akhmerov, and L. P. Kouwenhoven, Science **355**, 939 (2017).

[12] A. Imamoglu, H. Schmidt, G. Woods, and M. Deutsch, Phys. Rev. Lett. **79**, 1467 (1997).

[13] K. M. Birnbaum, A. Boca, R. Miller, A. D. Boozer, T. E. Northup, and H. J. Kimble, Nature (London) **436**, 87 (2005).

[14] J. M. Fink, A. Dombi, A. Vukics, A. Wallraff, and P. Domokos, Phys. Rev. X **7**, 011012 (2017).

[15] A. A. Sokolova, G. P. Fedorov, E. V. Il'ichev, and O. V. Astafiev, Phys. Rev. A **103**, 013718 (2021).

[16] A. Blais, A. L. Grimsmo, S. M. Girvin, and A. Wallraff, Rev. Mod. Phys. **93**, 025005 (2021).

[17] R. Barends, J. Kelly, A. Megrant, D. Sank, E. Jeffrey, Y. Chen, Y. Yin, B. Chiaro, J. Mutus, C. Neill *et al.*, Phys. Rev. Lett. **111**, 080502 (2013).

[18] G. Thomas, A. Gubaydullin, D. S. Golubev, and J. P. Pekola, Phys. Rev. B **102**, 104503 (2020).

[19] M. Löffler, G. M. Meyer, and H. Walther, Phys. Rev. A **55**, 3923 (1997).

[20] A. N. Bolgar, J. I. Zotova, D. D. Kirichenko, I. S. Besedin, A. V. Semenov, R. S. Shaikhaidarov, and O. V. Astafiev, Phys. Rev. Lett. **120**, 223603 (2018).

[21] J. Koch, T. M. Yu, J. Gambetta, A. A. Houck, D. I. Schuster, J. Majer, A. Blais, M. H. Devoret, S. M. Girvin, and R. J. Schoelkopf, Phys. Rev. A **76**, 042319 (2007).

[22] M. J. Peterer, S. J. Bader, X. Jin, F. Yan, A. Kamal, T. J. Gudmundsen, P. J. Leek, T. P. Orlando, W. D. Oliver, and S. Gustavsson, Phys. Rev. Lett. **114**, 010501 (2015).

[23] See Supplemental Material at http://link.aps.org/supplemental/10.1103/PhysRevA.107.L031701 for auxiliary experimental data, analytical/numerical models, and nanofabrication details.

[24] G. Fedorov and A. Ustinov, Quantum Sci. Technol. **4**, 045009 (2019).

[25] C. Wang, C. Axline, Y. Y. Gao, T. Brecht, Y. Chu, L. Frunzio, M. H. Devoret, and R. J. Schoelkopf, Appl. Phys. Lett. **107**, 162601 (2015).

[26] C. Cohen-Tannoudji, J. Dupont-Roc, and G. Grynberg, *Atom-Photon Interactions: Basic Processes and Applications* (Wiley, New York, 1998).

[27] G. P. Fedorov, V. B. Yursa, A. E. Efimov, K. I. Shiianov, A. Y. Dmitriev, I. A. Rodionov, A. A. Dobronosova, D. O. Moskalev, A. A. Pishchimova, E. I. Malevannaya, and O. V. Astafiev, Phys. Rev. A **102**, 013707 (2020).

[28] C. Buczek, R. Freiberg, and M. Skolnick, Proc. IEEE **61**, 1411 (1973).

[29] L. S. Bishop, J. M. Chow, J. Koch, A. A. Houck, M. H. Devoret, E. Thuneberg, S. M. Girvin, and R. J. Schoelkopf, Nat. Phys. **5**, 105 (2009).

[30] T. Hönigl-Decrinis, R. Shaikhaidarov, S. E. de Graaf, V. N. Antonov, and O. V. Astafiev, Phys. Rev. Appl. **13**, 024066 (2020).

[31] Y. Mu and C. M. Savage, Phys. Rev. A **46**, 5944 (1992).

[32] P. R. Rice and H. J. Carmichael, Phys. Rev. A **50**, 4318 (1994).

[33] Y.-Y. Liu, J. Stehlik, M. J. Gullans, J. M. Taylor, and J. R. Petta, Phys. Rev. A **92**, 053802 (2015).